Optik - International Journal for Light and Electron Optics 182 (2019) 555–564

Contents lists available at ScienceDirect

Optik

journal homepage: www.elsevier.com/locate/ijleo

Original research article

Numerical simulation of calibration algorithm based on inverse kinematics of the parallel mechanism

Liwei Yang[a,b,*], Xingzhi Tian[c], Zhilai Li[a], Fangmao Chai[a], Deyi Dong[a]

[a] Changchun Institute of Optics, Fine Mechanics and Physics, Chinese Academy of Sciences, Changchun, Jilin, 130033, China
[b] University of Chinese Academy of Sciences, Beijing, 100049, China
[c] Changchun Guanghua Microelectronic Equipment Engineering Center Co., Ltd, Changchun, Jilin, 130012, China

ARTICLE INFO

Keywords:
Parallel mechanism
Inverse kinematics
Error modeling
Calibration algorithm
Numerical simulation

ABSTRACT

This paper explores the numerical simulation of the calibration algorithm for the parallel mechanism with six degrees of freedoms (DOFs), aiming to verify the algorithm's robustness and effectiveness. Specifically, a Matlab-based numerical simulation method was proposed in light of the error modelling theory on inverse kinematics of the parallel mechanism. By this method, the actual poses are calculated through negative and forward kinematics models from the nominal values and errors of the parameters and several groups of nominal poses; then, the measuring uncertainty is introduced to derive the measured poses, and thus the pose errors; after that, the structural parameters are recognized by the least squares (LS) method, yielding the corrected values of the parameters; next, the corrected poses and pose errors were obtained through error compensation. The simulation results show that the positioning precision of the parallel mechanism was significantly improved through multiple iterations, indicating that the calibration algorithm is both robust and effective. The research findings lay a solid basis for subsequent calibration experiments.

1. Introduction

Recent years has seen a growing research interest in the calibration of kinematics parameters in parallel mechanism with six degrees of freedoms (DOFs). The actual parameters of the parallel mechanism may deviate from the theoretical ones, owing to the geometric errors in the manufacturing and assembly process. The resulting difference between the actual and nominal kinematics models in the motion control will lead to pose errors in the parallel mechanism.

Compared with the precision design, the kinematics calibration [1] is a posterior method to solve the said precision problem. If the mechanism is not manufactured or installed very precisely, this method can improve the precision of the mechanism without changing the hardware. Many studies have proved kinematics calibration as the most economical way to enhance mechanism precision.

By measurement outputs, the calibration can be divided into two categories: the self-calibration and the external calibration. The former constructs the error functional from the information acquired by the internal observer [2,3], and needs to install redundant sensors on the passive hinge (mounting an encoder on the Hooke's Joint, installing a grating scale on the mobile pair, etc.). The precision of the self-calibration is limited, because this method needs to find the forward solution of the calibration model and cannot

* Corresponding author at: Changchun Institute of Optics, Fine Mechanics and Physics, Chinese Academy of Sciences, Changchun, Jilin, 130033, China.
E-mail address: 13604415684@126.com (L. Yang).

https://doi.org/10.1016/j.ijleo.2019.01.079
Received 31 December 2018; Accepted 24 January 2019

acquire all the information of the end pose. The external calibration, however, constructs the error functional from the information collected by external measuring devices (e.g. laser range finder, laser interferometer and autocollimator). These devices are required to obtain the motion information of the parallel robot motion platform [4–6].

Much research has been done on the calibration and pose error compensation of the parallel mechanism, yielding many calibration and error compensation methods. For instance, Everett et al. [7] were the first to apply the self-calibration in closed-chain motion mechanism. After analyzing the source of calibration error, Judd et al. [8] considered non-geometric error as a major influencing factor of the calibration precision of the parallel mechanism. Zhuang et al. [9] constructed a simple calibration model in light of the structural features of the Stewart platform, which fixes the length of one branch to be identified and changes the length of other branches; nonetheless, this approach greatly reduces the measurable workspace. Patel A.J. et al. [10] created a parallel machine tool error model based on the Stewart platform, which can pinpoint all possible error sources. Considering the noisy environment of the machine tool, Chai et al. [11] put forward a simple, practical and robust way to calibrate the branch length. Ting et al. [12] proposed a three-point-three-axis calibration method. Pei Baoqing et al. [13] suggested analyzing the manufacturing and installation error and hinge gap error of the joints on the Stewart platform separately by fitting the error ellipsoid. Fazenda et al [14] measured Sigma 6 parallel mechanism by laser interferometer, photoelectron collimator and laser displacement sensor, and calibrated the mechanism by the neural network algorithm. Shi et al. [15] presented a calibration method using a laser interferometer and a self-collimator.

To sum up, the existing studies mainly concentrate on the error modeling and calibration methods for the parallel mechanism. However, there is virtually no report on the numerical simulation of calibration algorithm. As a key step before calibration tests, the numerical simulation is a drill of the entire calibration process, which helps to verify the validity and robustness of the calibration algorithm and to determine the measurement uncertainty of measuring instruments on the calibration precision.

In light of the above, this paper attempts to verify the robustness and effectiveness of the calibration algorithm for the 6-DOF parallel mechanism. To this end, the numerical simulation techniques of calibration algorithm were explored from the following aspects: the error modeling based on inverse kinematics (Section 2), the data processing based on the least squares (LS) method (Section 3), the evaluation indices of the calibration precision (Section 4) and the numerical simulation of calibration algorithm (Section 5).

2. Error modeling based on inverse kinematics

The kinematics calibration of the parallel mechanism includes four steps: error modeling, pose measurement, parameter identification and error compensation [1]. Among them, error modeling reflects the essence of the mechanism and lays the basis for the entire calibration process. In this paper, the error modeling is carried out based on inverse kinematics. The inverse kinematics refers to solving the length of the output branch according to the known pose of the end effector. For the 6-DOF parallel mechanism, the inverse kinematics is to determine the length $[l_1, l_2, l_3, l_4, l_5, l_6]^T$ of the six driving branches from the known pose $[X_P, Y_P, Z_P, \alpha, \beta, \gamma]^T$ of the motion platform.

In Fig. 1, $B_i(i = 1, 2,...,6)$ are the hinge points of the base platform, which fall on the same plane; $P_i(i = 1, 2,...,6)$ are the hinge points of the motion platform, which also fall on the same plane; $l_i(i = 1, 2,...,6)$ are the length of the branches; O -XYZ is the static coordinate system, with O being the geometric center of the base platform; P -XYZ is the dynamic coordinate system, with P being the geometric center of the motion platform.

In Fig. 2, O and P are the origins of the static coordinate system O-XYZ and the dynamic coordinate system P-XYZ, respectively; OP is the vector from the origin O of the static coordinate system to the origin P of the dynamic coordinate system; B_i are the vectors from the origin O of the static coordinate system to the position of each hinge point of the base platform; P_i are the vectors from the

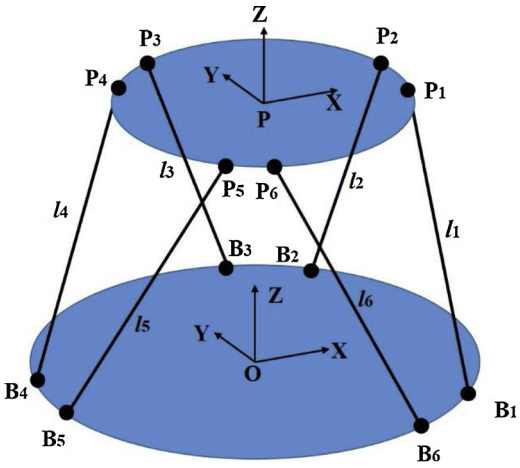

Fig. 1. Sketch map of the 6-DOF parallel mechanism.

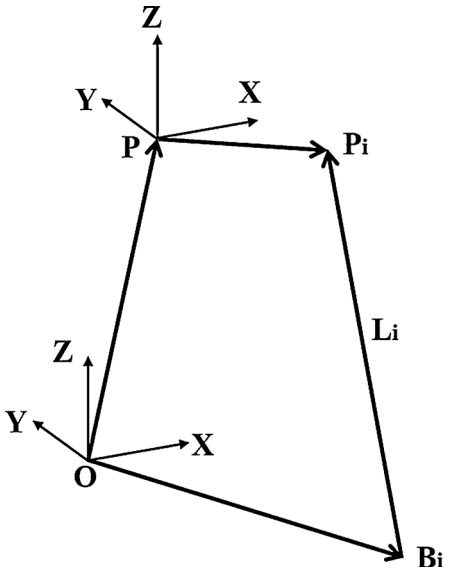

Fig. 2. Vectors related to the i-th branch.

origin P of the dynamic coordinate system to the position of each hinge point of the motion platform; L_i is the branch length vectors of the static coordinate system.

The branch length l_i of the static coordinate system can be obtained according to the closed-loop vector formula:

$$l_i = |L_i| = |\mathrm{R}^*\mathrm{P}_i + \mathrm{OP} - \mathrm{B}_i|, (\mathrm{i}=1, 2, \cdots, 6) \tag{1}$$

If sin and cos are abbreviated as s and c, respectively, then the R, P_i, OP and B_i in the above formula can be expressed as:

$$\mathrm{R}=\begin{bmatrix} c\alpha c\beta & c\alpha s\beta s\gamma - s\beta c\gamma & c\alpha s\beta c\gamma + s\alpha s\gamma \\ s\alpha b\beta & s\alpha s\beta s\gamma + c\alpha c\gamma & s\alpha s\beta c\gamma - c\alpha s\gamma \\ -s\beta & c\beta s\gamma & c\beta c\gamma \end{bmatrix} \tag{2}$$

$$P_i = [X_{Pi} \quad Y_{Pi} \quad Z_{Pi}]^T \tag{3}$$

$$OP = [X_P \quad Y_P \quad Z_P]^T \tag{4}$$

$$B_i = [X_{Bi} \quad Y_{Bi} \quad Z_{Bi}]^T \tag{5}$$

The length l_i of each driving branch can be obtained by substituting the mechanism parameters B_i and P_i as well as the pose parameters R and OP of the motion platform into formula (1), marking the end of the inverse kinematics.

Then, the nonlinear equations with unknown pose parameters of the motion platform can be derived from the inverse kinematics of the parallel mechanism:

$$|R^*P_i + OP - B_i|^2 - l_i^2 = 0, (i = 1, 2, \cdots, 6) \tag{6}$$

The above formula can be transformed into:

$$f_i(X_P, Y_P, Z_P, \alpha, \beta, \gamma, X_{Bi}, Y_{Bi}, Z_{Bi}, l_i, X_{Pi}, Y_{Pi}, Z_{Pi}) = 0, (i = 1, 2, \cdots, 6) \tag{7}$$

The manufacturing and installation errors of the mechanism components may cause errors in the six branches. Through complete differentiation, formula (7) can be transformed into:

$$\begin{aligned} &\frac{\partial f_i}{\partial X_P}dX_P + \frac{\partial f_i}{\partial Y_P}dY_P + \frac{\partial f_i}{\partial Z_P}dZ_P + \frac{\partial f_i}{\partial \alpha}d\alpha + \frac{\partial f_i}{\partial \beta}d\beta + \frac{\partial f_i}{\partial \gamma}d\gamma + \frac{\partial f_i}{\partial X_{Bi}}dX_{Bi} \\ &+ \frac{\partial f_i}{\partial Y_{Bi}}dY_{Bi} + \frac{\partial f_i}{\partial Z_{Bi}}dZ_{Bi} + \frac{\partial f_i}{\partial l_i}dl_i + \frac{\partial f_i}{\partial X_{Pi}}dX_{Pi} + \frac{\partial f_i}{\partial Y_{Pi}}dY_{Pi} + \frac{\partial f_i}{\partial Z_{Pi}}dZ_{Pi} = 0 \end{aligned} \tag{8}$$

Switching the last 7 terms to the right side, formula (8) can be written as the matrix below:

$$J \cdot dQ = B \tag{9}$$

where

$$J=\begin{bmatrix} \frac{\partial f_1}{\partial X_P} & \frac{\partial f_1}{\partial Y_P} & \frac{\partial f_1}{\partial Z_P} & \frac{\partial f_1}{\partial \alpha} & \frac{\partial f_1}{\partial \beta} & \frac{\partial f_1}{\partial \gamma} \\ \frac{\partial f_2}{\partial X_P} & \frac{\partial f_2}{\partial Y_P} & \frac{\partial f_2}{\partial Z_P} & \frac{\partial f_2}{\partial \alpha} & \frac{\partial f_2}{\partial \beta} & \frac{\partial f_2}{\partial \gamma} \\ \frac{\partial f_3}{\partial X_P} & \frac{\partial f_3}{\partial Y_P} & \frac{\partial f_3}{\partial Z_P} & \frac{\partial f_3}{\partial \alpha} & \frac{\partial f_3}{\partial \beta} & \frac{\partial f_3}{\partial \gamma} \\ \frac{\partial f_4}{\partial X_P} & \frac{\partial f_4}{\partial Y_P} & \frac{\partial f_4}{\partial Z_P} & \frac{\partial f_4}{\partial \alpha} & \frac{\partial f_4}{\partial \beta} & \frac{\partial f_4}{\partial \gamma} \\ \frac{\partial f_5}{\partial X_P} & \frac{\partial f_5}{\partial Y_P} & \frac{\partial f_5}{\partial Z_P} & \frac{\partial f_5}{\partial \alpha} & \frac{\partial f_5}{\partial \beta} & \frac{\partial f_5}{\partial \gamma} \\ \frac{\partial f_6}{\partial X_P} & \frac{\partial f_6}{\partial Y_P} & \frac{\partial f_6}{\partial Z_P} & \frac{\partial f_6}{\partial \alpha} & \frac{\partial f_6}{\partial \beta} & \frac{\partial f_6}{\partial \gamma} \end{bmatrix} \tag{10}$$

This is the Jacobian matrix of the nonlinear Eq. (6).

$$dQ=[dX_P \quad dY_P \quad dZ_P \quad d\alpha \quad d\beta \quad d\gamma]^T \tag{11}$$

This is the pose error resulted from the errors in structural parameters.

$$B=\begin{bmatrix} -\left(\frac{\partial f_1}{\partial X_{B1}}dX_{B1}+\frac{\partial f_1}{\partial Y_{B1}}dY_{B1}+\frac{\partial f_1}{\partial Z_{B1}}dZ_{B1}+\frac{\partial f_1}{\partial l_1}dl_1+\frac{\partial f_1}{\partial X_{P1}}dX_{P1}+\frac{\partial f_1}{\partial Y_{P1}}dY_{P1}+\frac{\partial f_1}{\partial Z_{P1}}dZ_{P1}\right) \\ -\left(\frac{\partial f_2}{\partial X_{B2}}dX_{B2}+\frac{\partial f_2}{\partial Y_{B2}}dY_{B2}+\frac{\partial f_2}{\partial Z_{B2}}dZ_{B2}+\frac{\partial f_2}{\partial l_2}dl_2+\frac{\partial f_2}{\partial X_{P2}}dX_{P2}+\frac{\partial f_2}{\partial Y_{P2}}dY_{P2}+\frac{\partial f_2}{\partial Z_{P2}}dZ_{P2}\right) \\ -\left(\frac{\partial f_3}{\partial X_{B3}}dX_{B3}+\frac{\partial f_3}{\partial Y_{B3}}dY_{B3}+\frac{\partial f_3}{\partial Z_{B3}}dZ_{B3}+\frac{\partial f_3}{\partial l_3}dl_3+\frac{\partial f_3}{\partial X_{P3}}dX_{P3}+\frac{\partial f_3}{\partial Y_{P3}}dY_{P3}+\frac{\partial f_3}{\partial Z_{P3}}dZ_{P3}\right) \\ -\left(\frac{\partial f_4}{\partial X_{B4}}dX_{B4}+\frac{\partial f_4}{\partial Y_{B4}}dY_{B4}+\frac{\partial f_4}{\partial Z_{B4}}dZ_{B4}+\frac{\partial f_4}{\partial l_4}dl_4+\frac{\partial f_4}{\partial X_{P4}}dX_{P4}+\frac{\partial f_4}{\partial Y_{P4}}dY_{P4}+\frac{\partial f_4}{\partial Z_{P5}}dZ_{P5}\right) \\ -\left(\frac{\partial f_5}{\partial X_{B5}}dX_{B5}+\frac{\partial f_5}{\partial Y_{B5}}dY_{B5}+\frac{\partial f_5}{\partial Z_{B5}}dZ_{B5}+\frac{\partial f_5}{\partial l_5}dl_5+\frac{\partial f_5}{\partial X_{P5}}dX_{P5}+\frac{\partial f_5}{\partial Y_{P5}}dY_{P5}+\frac{\partial f_5}{\partial Z_{P5}}dZ_{P5}\right) \\ -\left(\frac{\partial f_6}{\partial X_{B6}}dX_{B6}+\frac{\partial f_6}{\partial Y_{B6}}dY_{B6}+\frac{\partial f_6}{\partial Z_{B6}}dZ_{B6}+\frac{\partial f_6}{\partial l_6}dl_6+\frac{\partial f_6}{\partial X_{P6}}dX_{P6}+\frac{\partial f_6}{\partial Y_{P6}}dY_{P6}+\frac{\partial f_6}{\partial Z_{P6}}dZ_{P6}\right) \end{bmatrix} \tag{12}$$

Formula (9) is the error model of the 6-DOF parallel mechanism error model based on inverse kinematics. After measuring the pose data at each point, J can be deduced from formula (10), dQ can be directly obtained from the measured pose data, and B, which contains the above 42 independent error parameters, can be calculated by formula (9) from multiple sets of measured pose data.

3. LS-based parameter identification

Considering that each pose point can be described by 6 equations only, at least 7 sets of pose data should be measured to solve the 42 unknown parameters of the parallel mechanism. To ensure the rationality of the calibration results, more than 7 sets of pose data were measured to set up the function of the error between the actual and theoretical poses. After that, the motion parameters of the system were identified by the LS to obtain the error of the parallel mechanism. Finally, the parameters of the mechanism model were corrected to offset the error and complete the calibration. The LS can easily solve the unknown data and minimize the sum of squared errors of prediction (SSE) between the solution and the actual data.

A set of six equations can be established after measuring each set of pose data. Let n ($n \geq 7$) be the number of pose data sets. Then, a total of 6n equations, evenly distributed in n sets, can be established:

$$\begin{bmatrix} -\left(\frac{\partial f_1}{\partial X_{B1}}dX_{B1}+\frac{\partial f_1}{\partial Y_{B1}}dY_{B1}+\frac{\partial f_1}{\partial Z_{B1}}dZ_{B1}+\frac{\partial f_1}{\partial l_1}dl_1+\frac{\partial f_1}{\partial X_{P1}}dX_{P1}+\frac{\partial f_1}{\partial Y_{P1}}dY_{P1}+\frac{\partial f_1}{\partial Z_{P1}}dZ_{P1}\right) \\ -\left(\frac{\partial f_2}{\partial X_{B2}}dX_{B2}+\frac{\partial f_2}{\partial Y_{B2}}dY_{B2}+\frac{\partial f_2}{\partial Z_{B2}}dZ_{B2}+\frac{\partial f_2}{\partial l_2}dl_2+\frac{\partial f_2}{\partial X_{P2}}dX_{P2}+\frac{\partial f_2}{\partial Y_{P2}}dY_{P2}+\frac{\partial f_2}{\partial Z_{P2}}dZ_{P2}\right) \\ -\left(\frac{\partial f_3}{\partial X_{B3}}dX_{B3}+\frac{\partial f_3}{\partial Y_{B3}}dY_{B3}+\frac{\partial f_3}{\partial Z_{B3}}dZ_{B3}+\frac{\partial f_3}{\partial l_3}dl_3+\frac{\partial f_3}{\partial X_{P3}}dX_{P3}+\frac{\partial f_3}{\partial Y_{P3}}dY_{P3}+\frac{\partial f_3}{\partial Z_{P3}}dZ_{P3}\right) \\ -\left(\frac{\partial f_4}{\partial X_{B4}}dX_{B4}+\frac{\partial f_4}{\partial Y_{B4}}dY_{B4}+\frac{\partial f_4}{\partial Z_{B4}}dZ_{B4}+\frac{\partial f_4}{\partial l_4}dl_4+\frac{\partial f_4}{\partial X_{P4}}dX_{P4}+\frac{\partial f_4}{\partial Y_{P4}}dY_{P4}+\frac{\partial f_4}{\partial Z_{P5}}dZ_{P5}\right) \\ -\left(\frac{\partial f_5}{\partial X_{B5}}dX_{B5}+\frac{\partial f_5}{\partial Y_{B5}}dY_{B5}+\frac{\partial f_5}{\partial Z_{B5}}dZ_{B5}+\frac{\partial f_5}{\partial l_5}dl_5+\frac{\partial f_5}{\partial X_{P5}}dX_{P5}+\frac{\partial f_5}{\partial Y_{P5}}dY_{P5}+\frac{\partial f_5}{\partial Z_{P5}}dZ_{P5}\right) \\ -\left(\frac{\partial f_6}{\partial X_{B6}}dX_{B6}+\frac{\partial f_6}{\partial Y_{B6}}dY_{B6}+\frac{\partial f_6}{\partial Z_{B6}}dZ_{B6}+\frac{\partial f_6}{\partial l_6}dl_6+\frac{\partial f_6}{\partial X_{P6}}dX_{P6}+\frac{\partial f_6}{\partial Y_{P6}}dY_{P6}+\frac{\partial f_6}{\partial Z_{P6}}dZ_{P6}\right) \end{bmatrix}_{Aj} = \begin{bmatrix} \frac{\partial f_1}{\partial X_P} & \frac{\partial f_1}{\partial Y_P} & \frac{\partial f_1}{\partial Z_P} & \frac{\partial f_1}{\partial \alpha} & \frac{\partial f_1}{\partial \beta} & \frac{\partial f_1}{\partial \gamma} \\ \frac{\partial f_2}{\partial X_P} & \frac{\partial f_2}{\partial Y_P} & \frac{\partial f_2}{\partial Z_P} & \frac{\partial f_2}{\partial \alpha} & \frac{\partial f_2}{\partial \beta} & \frac{\partial f_2}{\partial \gamma} \\ \frac{\partial f_3}{\partial X_P} & \frac{\partial f_3}{\partial Y_P} & \frac{\partial f_3}{\partial Z_P} & \frac{\partial f_3}{\partial \alpha} & \frac{\partial f_3}{\partial \beta} & \frac{\partial f_3}{\partial \gamma} \\ \frac{\partial f_4}{\partial X_P} & \frac{\partial f_4}{\partial Y_P} & \frac{\partial f_4}{\partial Z_P} & \frac{\partial f_4}{\partial \alpha} & \frac{\partial f_4}{\partial \beta} & \frac{\partial f_4}{\partial \gamma} \\ \frac{\partial f_5}{\partial X_P} & \frac{\partial f_5}{\partial Y_P} & \frac{\partial f_5}{\partial Z_P} & \frac{\partial f_5}{\partial \alpha} & \frac{\partial f_5}{\partial \beta} & \frac{\partial f_5}{\partial \gamma} \\ \frac{\partial f_6}{\partial X_P} & \frac{\partial f_6}{\partial Y_P} & \frac{\partial f_6}{\partial Z_P} & \frac{\partial f_6}{\partial \alpha} & \frac{\partial f_6}{\partial \beta} & \frac{\partial f_6}{\partial \gamma} \end{bmatrix}_{Aj} \begin{bmatrix} dX_P \\ dY_P \\ dZ_P \\ d\alpha \\ d\beta \\ d\gamma \end{bmatrix}_{Aj} \tag{13}$$

where Aj (j = 1, 2, 3,..., n) are n pose measuring positions; $\frac{\partial f_i}{\partial X_{Bi}}$, $\frac{\partial f_i}{\partial Y_{Bi}}$, $\frac{\partial f_i}{\partial Z_{Bi}}$, $\frac{\partial f_i}{\partial l_i}$, $\frac{\partial f_i}{\partial X_{Pi}}$, $\frac{\partial f_i}{\partial Y_{Pi}}$, $\frac{\partial f_i}{\partial Z_{Pi}}$, $\frac{\partial f_i}{\partial X_P}$, $\frac{\partial f_i}{\partial Y_P}$, $\frac{\partial f_i}{\partial Z_P}$, $\frac{\partial f_i}{\partial \alpha}$, $\frac{\partial f_i}{\partial \beta}$, $\frac{\partial f_i}{\partial \gamma}$, dX_P, dY_P, dZ_P, $d\alpha$, $d\beta$ and $d\gamma$ (i = 1,2,3,..., 6) are the data acquired by pose measurement at each measuring position; dX_{Bi}, dY_{Bi}, dZ_{Bi}, dl_i, dX_{Pi}, dY_{Pi} and dZ_{Pi} (i = 1,2,3,..., 6) are the unknown error parameters acquired by pose measurement at each measuring position. In total, 84 data and 42 unknown error parameters were acquired by pose measurement.

The 6n equations can be integrated into 6 sets of equations, each of which contains n equations:

$$\begin{bmatrix} -\left(\frac{\partial f_i}{\partial X_{Bi}}dX_{Bi}+\frac{\partial f_i}{\partial Y_{Bi}}dY_{Bi}+\frac{\partial f_i}{\partial Z_{Bi}}dZ_{Bi}+\frac{\partial f_i}{\partial l_i}dl_i+\frac{\partial f_i}{\partial X_{Pi}}dX_{Pi}+\frac{\partial f_i}{\partial Y_{Pi}}dY_{Pi}+\frac{\partial f_i}{\partial Z_{Pi}}dZ_{Pi}\right)_{A1} \\ -\left(\frac{\partial f_i}{\partial X_{Bi}}dX_{Bi}+\frac{\partial f_i}{\partial Y_{Bi}}dY_{Bi}+\frac{\partial f_i}{\partial Z_{Bi}}dZ_{Bi}+\frac{\partial f_i}{\partial l_i}dl_i+\frac{\partial f_i}{\partial X_{Pi}}dX_{Pi}+\frac{\partial f_i}{\partial Y_{Pi}}dY_{Pi}+\frac{\partial f_i}{\partial Z_{Pi}}dZ_{Pi}\right)_{A2} \\ -\left(\frac{\partial f_i}{\partial X_{Bi}}dX_{Bi}+\frac{\partial f_i}{\partial Y_{Bi}}dY_{Bi}+\frac{\partial f_i}{\partial Z_{Bi}}dZ_{Bi}+\frac{\partial f_i}{\partial l_i}dl_i+\frac{\partial f_i}{\partial X_{Pi}}dX_{Pi}+\frac{\partial f_i}{\partial Y_{Pi}}dY_{Pi}+\frac{\partial f_i}{\partial Z_{Pi}}dZ_{Pi}\right)_{A3} \\ -\left(\frac{\partial f_i}{\partial X_{Bi}}dX_{Bi}+\frac{\partial f_i}{\partial Y_{Bi}}dY_{Bi}+\frac{\partial f_i}{\partial Z_{Bi}}dZ_{Bi}+\frac{\partial f_i}{\partial l_i}dl_i+\frac{\partial f_i}{\partial X_{Pi}}dX_{Pi}+\frac{\partial f_i}{\partial Y_{Pi}}dY_{Pi}+\frac{\partial f_i}{\partial Z_{Pi}}dZ_{Pi}\right)_{A4} \\ \vdots \\ -\left(\frac{\partial f_i}{\partial X_{Bi}}dX_{Bi}+\frac{\partial f_i}{\partial Y_{Bi}}dY_{Bi}+\frac{\partial f_i}{\partial Z_{Bi}}dZ_{Bi}+\frac{\partial f_i}{\partial l_i}dl_i+\frac{\partial f_i}{\partial X_{Pi}}dX_{Pi}+\frac{\partial f_i}{\partial Y_{Pi}}dY_{Pi}+\frac{\partial f_i}{\partial Z_{Pi}}dZ_{Pi}\right)_{An} \end{bmatrix}$$

$$= \begin{bmatrix} \left(\frac{\partial f_i}{\partial X_P}dX_P+\frac{\partial f_i}{\partial Y_P}dY_P+\frac{\partial f_i}{\partial Z_P}dZ_P+\frac{\partial f_i}{\partial \alpha}d\alpha+\frac{\partial f_i}{\partial \beta}d\beta+\frac{\partial f_i}{\partial \gamma}d\gamma\right)_{A1} \\ \left(\frac{\partial f_i}{\partial X_P}dX_P+\frac{\partial f_i}{\partial Y_P}dY_P+\frac{\partial f_i}{\partial Z_P}dZ_P+\frac{\partial f_i}{\partial \alpha}d\alpha+\frac{\partial f_i}{\partial \beta}d\beta+\frac{\partial f_i}{\partial \gamma}d\gamma\right)_{A2} \\ \left(\frac{\partial f_i}{\partial X_P}dX_P+\frac{\partial f_i}{\partial Y_P}dY_P+\frac{\partial f_i}{\partial Z_P}dZ_P+\frac{\partial f_i}{\partial \alpha}d\alpha+\frac{\partial f_i}{\partial \beta}d\beta+\frac{\partial f_i}{\partial \gamma}d\gamma\right)_{A3} \\ \left(\frac{\partial f_i}{\partial X_P}dX_P+\frac{\partial f_i}{\partial Y_P}dY_P+\frac{\partial f_i}{\partial Z_P}dZ_P+\frac{\partial f_i}{\partial \alpha}d\alpha+\frac{\partial f_i}{\partial \beta}d\beta+\frac{\partial f_i}{\partial \gamma}d\gamma\right)_{A4} \\ \vdots \\ \left(\frac{\partial f_i}{\partial X_P}dX_P+\frac{\partial f_i}{\partial Y_P}dY_P+\frac{\partial f_i}{\partial Z_P}dZ_P+\frac{\partial f_i}{\partial \alpha}d\alpha+\frac{\partial f_i}{\partial \beta}d\beta+\frac{\partial f_i}{\partial \gamma}d\gamma\right)_{An} \end{bmatrix} \tag{14}$$

where i = 1, 2, …, 6 are the six branches of the parallel mechanism; A1, A2,…, An are the n pose measuring positions. Each set of equations only has one error parameters of the branch. Solving each set by the LS, it is possible to determine the error parameters of the parallel mechanism.

4. Evaluation indices of calibration precision

The precision evaluation indices are responsible to express the kinematics error of the mechanism and demonstrate the calibration effect during the calibration of mechanism error parameters. As a result, the following two issues must be considered for the rational design of precision evaluation indices: First, the magnitude and impact of the errors should be depicted in a comprehensive and accurate manner, after full consideration of the distribution of mechanism errors in the 6D pose space; Second, the calibration results should be evaluated scientifically, rigorously and conveniently. In view of the features of pose errors and the form of pose information in the 6-DOF parallel mechanism, this paper designs the precision evaluation indies through the following two steps.

4.1. Determination of the integrated error

The original pose error dQ was derived from the pose information acquired at a measuring point in the workspace. Then, the position error, the orientation error and the integrated error can be calculated by Formulas (15), (16) and (17), respectively.

$$dQ_1 = \left|\left[dX_P \quad dY_P \quad dZ_P\right]^T\right|_2 = \sqrt{dX_P^2 + dY_P^2 + dZ_P^2} \tag{15}$$

$$dQ_2 = \left|\left[d\alpha \quad d\beta \quad d\gamma\right]^T\right|_2 = \sqrt{d\alpha^2 + d\beta^2 + d\gamma^2} \tag{16}$$

$$dQ_{\text{int}} = dQ_1 + dQ_2 \tag{17}$$

The modulus of the position error and orientation error at the measuring point, defined in the form of 2-norm, can clearly reflect the kinematics error of the 6-DOF parallel mechanism at this point [9].

4.2. Balance between the error components

The components dQ_1 and dQ_2 in the original error dQ_{int} should be balanced, i.e., the magnitude of the position error and the orientation error in the original error should be balanced, while dQ_1 and dQ_2 are being reduced. In other words, the numerical difference between dX_P, dY_P and dZ_P as well as that between $d\alpha$, $d\beta$ and $d\gamma$ must be controlled to a small value.

5. Numerical simulation of calibration algorithm

Before calibrating the parallel mechanism, it is necessary to numerically simulate the error compensation and calibration. The simulation aims to verify the robustness and effectiveness of the calibration algorithm. For simplicity, the definitions of the symbols used in the numerical simulation are listed in Table 1 below.

The numerical simulation adopts the following program:

Table 1
Symbol definitions.

Serial No.	Parameter symbol	Definition
1	Q_N	Nominal pose
2	B_N	Nominal lower hinge parameter
3	P_N	Nominal upper hinge parameter
4	l_N	Nominal branch length
5	d B_N	Lower hinge parameter error
6	d P_N	Upper hinge parameter error
7	d l_N	Branch length error
8	B_A	Actual lower hinge parameter
9	P_A	Actual upper hinge parameter
10	l_A	Actual branch length
11	Q_A	Actual pose
12	σ	Measuring uncertainty
13	Q_M	Measured pose
14	dQ	Pose error
15	d B_C’	Unknown lower hinge parameter error
16	d P_C’	Unknown upper hinge parameter error
17	d l_C’	Unknown branch length error
18	B_C	Corrected lower hinge parameter
19	P_C	Corrected upper hinge parameter
20	l_C	Corrected branch length
21	Q_C	Corrected pose
22	dQ_C	Corrected pose error
23	dQ_{int}	Integrated error
24	ε	Iterative tolerance

(1) Initialize the nominal poses QN, nominal parameters BN and PN, and errors d BN, d PN and d lN of the 6-DOF parallel mechanism.
(2) Calculate the actual poses QA: Determine the nominal branch lengths lN by substituting the given nominal poses QN, nominal parameters BN and PN, and errors d BN, d PN and d lN into the inverse kinematics formula of the 6-DOF parallel mechanism. Next, derive the actual hinge parameters BA and PA and actual branch lengths lA from the given hinge parameter errors d BN and d PN and the branch length errors d lN. After that, compute the actual poses QA by the forward kinematics formula.
(3) Calculate the measured poses QM: Obtain the measured poses QM after introducing the measuring uncertainty σ.
(4) Calculate the pose errors dQ : Obtain the pose errors dQ through the subtraction between the measured poses QM and the nominal poses QN.
(5) Recognize parameter errors: Obtain the parameter errors d BC’, d PC’ and d lC’ through LS processing of the above data.
(6) Compensate for the errors: Obtain the corrected parameters BC, PC and lC by adding parameter errors to the corresponding nominal parameters, thus completing error compensation.
(7) Calculate corrected poses Qc: Obtain the corrected poses by substituting the corrected parameters into the forward kinematics formula.
(8) Calculate corrected pose errors dQc: Obtain the corrected pose errors through the subtraction between the measured poses QM and the corrected poses QC.
(9) Judge whether the corrected errors meet the requirements: Calculate integrated error $dQ_{\text{int}}^{j}(j = 1, 2, \cdots n)$. If $\max_{1\le j\le n}(dQ_{\text{int}}^{j}) \le \varepsilon$, terminate the iteration and take the current parameters BC, PC and lC as the actual structure parameters of the mechanism; otherwise, go to Step 10.
(10) Replace dQ with dQC and return to Step 5, and repeat the above steps until $\max_{1\le j\le n}(dQ_{\text{int}}^{j}) \le \varepsilon$.

The entire numerical simulation process is illustrated in Fig. 3 below.

After iterative calculation, the latest parallel mechanism parameters were obtained. These parameters can be viewed as the actual structural parameters of the mechanism. Then, the parallel mechanism parameters in the control program were corrected according to the calculation results, thereby offsetting the error and improving the positioning precision of the mechanism.

5.1. Determining the nominal kinematics parameter errors

A digital model was established for the 6-DOF parallel mechanism. The 42 kinematic parameters of the mechanism 42 are shown in Table 2, and the errors of these parameters are assumed as shown in Table 3.

5.2. Generating analog measured data

Ten poses were selected from the workspace (Table 4) and imported to the inverse kinematics model with error-free diving

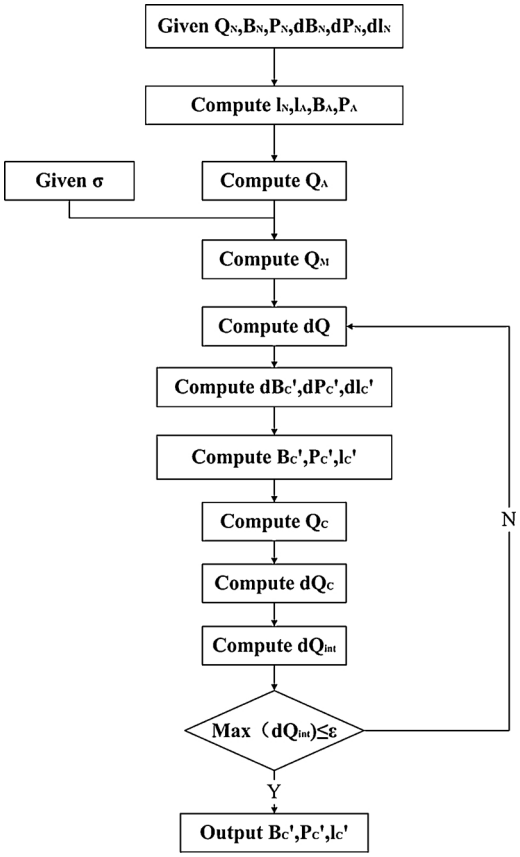

Fig. 3. Flow chart of numerical simulation.

Table 2
Nominal values of 42 kinematic parameters.

Branch 1#	X_{B1}	Y_{B1}	Z_{B1}	l_1	X_{P1}	Y_{P1}	Z_{P1}
	120	−140	0	233.23808	120	−20	0
Branch 2#	X_{B2}	Y_{B2}	Z_{B2}	l_2	X_{P2}	Y_{P2}	Z_{P2}
	120	140	0	233.23808	120	20	0
Branch 3#	X_{B3}	Y_{B3}	Z_{B3}	l_3	X_{P3}	Y_{P3}	Z_{P3}
	61.243557	173.92305	0	233.23808	−42.679489	113.92304	0
Branch 4#	X_{B4}	Y_{B4}	Z_{B4}	l_4	X_{P4}	Y_{P4}	Z_{P4}
	−181.24356	33.92305	0	233.23808	−77.320511	93.923042	0
Branch 5#	X_{B5}	Y_{B5}	Z_{B5}	l_5	X_{P5}	Y_{P5}	Z_{P5}
	−181.24356	−33.92305	0	233.23808	−77.320511	−93.923042	0
Branch 6#	X_{B6}	Y_{B6}	Z_{B6}	l_6	X_{P6}	Y_{P6}	Z_{P6}
	61.243557	−173.92305	0	233.23808	−42.679489	−113.92304	0

Table 3
Errors in the 42 kinematic parameters.

Branch 1#	dX_{B1}	dY_{B1}	dZ_{B1}	dl_1	dX_{P1}	dY_{P1}	dZ_{P1}
	0.02	0.03	−0.05	−0.02	0.04	0.03	−0.01
Branch 2#	dX_{B2}	dY_{B2}	dZ_{B2}	dl_2	dX_{P2}	dY_{P2}	dZ_{P2}
	−0.03	0.02	0.04	0.02	0.05	−0.02	−0.03
Branch 3#	dX_{B3}	dY_{B3}	dZ_{B3}	dl_3	dX_{P3}	dY_{P3}	dZ_{P3}
	0.01	−0.05	0.04	−0.01	−0.02	0.01	0.04
Branch 4#	dX_{B4}	dY_{B4}	dZ_{B4}	dl_4	dX_{P4}	dY_{P4}	dZ_{P4}
	−0.05	−0.02	0.02	0.04	−0.04	−0.04	0.01
Branch 5#	dX_{B5}	dY_{B5}	dZ_{B5}	dl_5	dX_{P5}	dY_{P5}	dZ_{P5}
	−0.02	0.05	−0.01	−0.05	0.04	0.02	−0.05
Branch 6#	dX_{B6}	dY_{B6}	dZ_{B6}	dl_6	dX_{P6}	dY_{P6}	dZ_{P6}
	0.05	−0.04	−0.02	0.04	0.02	0.03	0.04

Table 4
Pose data selected from the workspace.

		X(mm)	Y(mm)	Z(mm)	α(rad)	β(rad)	γ(rad)
A1	P_T	10	0	200	0.017453292	0.034907	0.05236
	P_P	10.02907	−0.04008	199.991	0.017814	0.034796	0.051874
	$E_1 = P_P\text{-}P_T$	0.02907	−0.04008	−0.009	0.000360708	−0.00011	−0.00049
A2	P_T	10	10	200	0.034906584	−0.03491	0.017453
	P_P	10.0562	9.9385	199.9848	0.0352	−0.035	0.0174
	$E_1 = P_P\text{-}P_T$	0.0562	−0.0615	−0.0152	0.000293416	−0.0000934	−0.0000533
A3	P_T	0	10	200	0.052359877	0.034907	−0.01745
	P_P	0.040607	9.958774	199.9928	0.052729	0.034775	−0.01794
	$E_1 = P_P\text{-}P_T$	0.040607	−0.04123	−0.0072	0.000369123	−0.00013	−0.00049
A4	P_T	−10	10	200	−0.05235988	−0.01745	0.017453
	P_P	−9.96499	9.955117	199.9963	−0.05197	−0.0176	0.016979
	$E_1 = P_P\text{-}P_T$	0.03501	−0.04488	−0.0037	0.000389877	−0.00015	−0.00047
A5	P_T	−10	0	200	−0.01745329	0.017453	0.034907
	P_P	−9.96692	−0.04496	199.9954	−0.01707	0.017326	0.034433
	$E_1 = P_P\text{-}P_T$	0.03308	−0.04496	−0.0046	0.000383292	−0.00013	−0.00047
A6	P_T	−10	−10	200	0.017453292	−0.05236	0.017453
	P_P	−9.96952	−10.0419	199.9906	0.01787	−0.05245	0.016936
	$E_1 = P_P\text{-}P_T$	0.03048	−0.0419	−0.0094	0.000416708	−9E-05	−0.00052
A7	P_T	0	−10	200	0.034906584	0.05236	−0.03491
	P_P	0.03019	−10.0384	199.9892	0.035264	0.052294	−0.03537
	$E_1 = P_P\text{-}P_T$	0.03019	−0.0384	−0.0108	0.000357416	−6.6E-05	−0.00046
A8	P_T	10	−10	200	0.052359877	0.017453	0.05236
	P_P	10.02686	−10.0388	199.9887	0.052733	0.017372	0.051853
	$E_1 = P_P\text{-}P_T$	0.02686	−0.0388	−0.0113	0.000373123	−8.1E-05	−0.00051
A9	P_T	0	0	210	−0.03490658	0.034907	−0.05236
	P_P	0.031535	−0.04165	209.9913	−0.03457	0.034827	−0.05282
	$E_1 = P_P\text{-}P_T$	0.031535	−0.04165	−0.0087	0.000336584	−8E-05	−0.00046
A10	P_T	0	0	210	0.034906584	−0.03491	0.034907
	P_P	0.034993	−0.04456	209.9916	0.035298	−0.03502	0.034362
	$E_1 = P_P\text{-}P_T$	0.034993	−0.04456	−0.0084	0.000391416	−0.00011	−0.00054

parameters, thereby finding the theoretical driving parameters of each branch. The theoretical parameters were inputted into the error-containing forward kinematics model, yielding the actual poses of the motion platform. On this basis, a random error within ± 0.001 mm was added to simulate the measuring uncertainty caused by the controller, the measuring instruments and environmental factors. After the addition, the data were adopted as the analog measured data (Table 4).

5.3. Initializing iteration positioning error

The analog measured pose data were compared with the nominal pose data to obtain the initial positioning error (Table 4).

5.4. Iterative solution

The positioning error was substituted into the set of equations in the calibration model of the parallel mechanism. Then, the set of equations were solved through Matlab program, yielding 42 unknown error coefficients. Through the iterative calculation, the

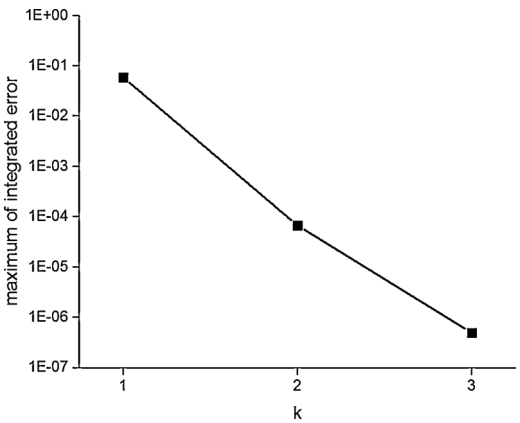

Fig. 4. Iteration curve.

Table 5
Comparison of parameter errors before and after calibration (unit: mm).

Branch 1#		dX_{B1}	dY_{B1}	dZ_{B1}	dl_1	dX_{P1}	dY_{P1}	dZ_{P1}
	before	0.02	0.03	−0.05	−0.02	0.04	0.03	−0.01
	after (*e-3)	−0.0016	0.4274	0.7004	−0.8464	0.0016	−0.0123	−0.0237
Branch 2#		dX_{B2}	dY_{B2}	dZ_{B2}	dl_2	dX_{P2}	dY_{P2}	dZ_{P2}
	before	−0.03	0.02	0.04	0.02	0.05	−0.02	−0.03
	after (*e-3)	−0.0098	−0.2020	0.3315	−0.3144	0.0056	−0.0452	0.0588
Branch 3#		dX_{B3}	dY_{B3}	dZ_{B3}	dl_3	dX_{P3}	dY_{P3}	dZ_{P3}
	before	0.01	−0.05	0.04	−0.01	−0.02	0.01	0.04
	after (*e-3)	−0.1447	−0.0758	0.2493	−0.4092	0.0494	0.0204	−0.0985
Branch 4#		dX_{B4}	dY_{B4}	dZ_{B4}	dl_4	dX_{P4}	dY_{P4}	dZ_{P4}
	before	−0.05	−0.02	0.02	0.04	−0.04	−0.04	0.01
	after (*e-3)	0.1426	0.0957	0.3049	−0.1162	0.104	0.067	0.1984
Branch 5#		dX_{B5}	dY_{B5}	dZ_{B5}	dl_5	dX_{P5}	dY_{P5}	dZ_{P5}
	before	−0.02	0.05	−0.01	−0.05	0.04	0.02	−0.05
	after (*e-3)	0.1309	−0.0577	0.2294	0.0607	0.1569	−0.0691	0.2837
Branch 6#		dX_{B6}	dY_{B6}	dZ_{B6}	dl_6	dX_{P6}	dY_{P6}	dZ_{P6}
	before	0.05	−0.04	−0.02	0.04	0.02	0.03	0.04
	after (*e-3)	−0.117	0.0603	0.2108	−0.2272	0.01	−0.0135	−0.0244

theoretical values of 42 kinematics parameters were continuously corrected until the terminal condition $\max_{1\le j\le n}(dQ_{\text{int}}^{j}) \le \varepsilon = 1\times 10^{-6}$ was fulfilled. As shown in Fig. 4, $\max_{1\le j\le n}(dQ_{\text{int}}^{j})$ dropped below the termination condition after 2 iterations, thus ending the iteration. At this time, the 42 kinematics parameters converged to the corresponding actual values one by one. Each actual value is the algebraic sum of the nominal parameter value and the unknown parameter error.

For better understanding of the variation of the kinematics parameters in the iteration, Table 5 compares the pre- and post-calibration errors of each kinematic parameter. The initial error of each parameter was determined by the difference between the actual and nominal values of the parameter. The difference is given in Step (1) of the numerical simulation. The final error of each parameter was determined by the difference between the actual value of the parameter and the value under the termination condition. As shown in Table 5, the errors of most parameters decreased significantly after the iterative calibration, indicating that the LS-based calibration works correctly for the kinematic parameters. It should be noted that parameter errors are inevitable even with multiple iterations, because the actual measurement and the iterative calculation will lead to additional errors.

Table 6 compares the poses errors before and after the calibration. It can be seen that the positioning precision of the parallel mechanism was significantly improved through the calibration. This means the calibration algorithm can effectively enhance the pose precision of the mechanism. Similar to parameter errors, the pose errors cannot be fully eliminated despite multiple iterations, because additional errors will occur in the actual measurement and the iterative calculation.

6. Conclusions

This paper explores the numerical simulation of calibration algorithm for the 6-DOF parallel mechanism, in an attempt to verify

Table 6
Comparison of pose errors before and after calibration.

		dX(mm)	dY(mm)	dZ(mm)	dα(mrad)	dβ(mrad)	dγ(mrad)
A1	before	0.02907	−0.04008	−0.009	0.000360708	−0.00011	−0.00049
	after	4.85E-07	4.00E-08	3.37E-07	−1.52E-10	−2.92E-10	−2.01E-10
A2	before	0.0562	−0.0615	−0.0152	0.000293416	−0.0000934	−0.0000533
	after	−6.68E-08	−4.00E-07	−2.98E-07	4.06E-10	−1.65E-09	−1.77E-09
A3	before	0.040607	−0.04123	−0.0072	0.000369123	−0.00013	−0.00049
	after	−2.87E-09	−1.39E-08	5.17E-07	−3.64E-10	1.19E-09	5.74E-10
A4	before	0.03501	−0.04488	−0.0037	0.000389877	−0.00015	−0.00047
	after	4.01E-07	−9.99E-08	−2.29E-07	−2.55E-11	−5.39E-10	−9.22E-10
A5	before	0.03308	−0.04496	−0.0046	0.000383292	−0.00013	−0.00047
	after	−5.59E-08	−2.93E-08	−8.94E-08	6.45E-10	−6.79E-10	6.67E-10
A6	before	0.03048	−0.0419	−0.0094	0.000416708	−9.00E-05	−0.00052
	after	−2.61E-07	−3.08E-07	3.34E-07	−1.54E-09	3.24E-10	1.87E-09
A7	before	0.03019	−0.0384	−0.0108	0.000357416	−6.60E-05	−0.00046
	after	2.39E-08	−4.08E-07	−5.91E-07	5.92E-10	−1.14E-09	−1.06E-09
A8	before	0.02686	−0.0388	−0.0113	0.000373123	−8.10E-05	−0.00051
	after	8.91E-08	4.18E-07	−5.91E-08	1.20E-09	8.06E-10	−4.49E-12
A9	before	0.031535	−0.04165	−0.0087	0.000336584	−8.00E-05	−0.00046
	after	−5.92E-07	2.22E-07	1.39E-07	−3.87E-10	1.70E-10	8.43E-10
A10	before	0.034993	−0.04456	−0.0084	0.000391416	−0.00011	−0.00054
	after	1.25E-08	5.16E-07	−7.75E-08	−3.91E-10	1.57E-09	9.54E-11

the algorithm's robustness and effectiveness. Firstly, the composition of the 6-DOF parallel mechanism was introduced, and a calibration algorithm was proposed based on inverse kinematics. Inspired by the LS, the algorithm tries to find the 42 main kinematics parameters of the 6-DOF parallel mechanism. Then, the solution process of the calibration algorithm was discussed in details, and the algorithm was verified by computer simulation. The simulation results show that the parallel mechanism enjoyed better pose precision after its kinematics parameters were calibrated by our algorithm. This means the proposed algorithm is both robust and effective, laying a solid basis for subsequent calibration experiments.

Acknowledgement

The author(s) disclosed receipt of the following financial support for the research and/or authorship of this article: This work is supported by the National Key Research and Development Program (No.2016YFB0500100) and by the National Natural Science Foundation of China (No.11873007).

References

[1] ZviS. Roth, Bahram Ravani, et al., An overview of robot calibration, IEEE J. Robot. Autom. 3 (5) (1987) 377–385.
[2] A. Rauf, J. Ryu, Fully Autonomous calibration of parallel manipulators by imposing positon constraint, Proceedings of IEEE International Conference on Robotics and Automation (2001) 2389–2394.
[3] Y.K. Liu, J. Meng, Z.X. Li, Auto-calibration for a parallel manipulator with sensor redundancy, Proceedings of IEEE International Conference on Robotics and Automation.Taipei, (2003), pp. 3660–3665.
[4] T. Huang, D.G. Chetwynd, D.D. Whitehouse, et al., A general and novel approach for parameter identification of 6-DOF parallel kinematic machines, Mech. Mach. Theory 40 (2) (2005) 219–239.
[5] S. Besnard, W. Khalil, Calibration of parallel robots using Two inclinometers, Proceedings of IEEE International Conference on Robotics and Automation (1999) 1758–1763.
[6] D. Daney, I.Z. Emiris, Robust parallel robot calibration with partial information, Proceedings of IEEE International Conference on Robotics and Automation (2001) 3262–3267.
[7] L.J. Everett, M. Driels, B.W. Mooring, IEEE XploreKinematic Modeling for Robot Calibration[C]// IEEE International Conference on Robotics and Automation. Proceedings1987, Kinematic Modeling for Robot Calibration[C]// IEEE International Conference on Robotics and Automation. Proceedings (1987) 183–189.
[8] R.P. Judd, A.B. Knasinski, A technique to calibrate industrial robots with experimental verification[J], IEEE Trans Robot. Autom. 6 (1) (1987) 20–30.
[9] H. Zhuang, Z.S. Roth, Method for Kinematic Calibration of Stewart Platforms[C]// Proc.1991 ASME Ann.Winter Meeting, (1993), pp. 391–405.
[10] A.J. Patel, K.F. Ehmann, Volumetric error analysis of a Stewart platform-based machine tool, CIRP Ann. Manuf. Technol. 46 (1) (1997) 287–290.
[11] K.S. Chai, K. Young, I. Tuersley, A Practical Calibration Process Using Partial Information For A Commercial Stewart Platform Vol 20 Cambridge University Press, 2002, pp. 315–322 (3).
[12] Y. Ting, H.C. Jar, C.C. Li, IEEEError Compensation and Feedforward Controller Design for a 6-Dof Micro-Positioning Platform[C]// IEEE/Rsj International Conference on Intelligent Robots and Systems2005, Error Compensation and Feedforward Controller Design for a 6-Dof Micro-Positioning Platform[C]// IEEE/Rsj International Conference on Intelligent Robots and Systems (2005) 942–947.
[13] B.P. PEI, W.Y. CHEN, T.M. WANG, Calibration and analysis of joints position and clearance error on 6UPS parallel machine, Mach. Design Res. (9) (2005) 49–51.
[14] N. Fujisawa, K. Itonaga, S. Maeno, Calibration of the 6 DOF high-precision flexure parallel, robot "Sigma 6", Parallel Kinematic Mach. Res. Pract. 2002 (2) (2006) 659–660.
[15] H. Shi, H.J. Su, N. Dagalakis, et al., Kinematic modeling and calibration of a flexure based hexapod nanopositioner, Precis. Eng. 37 (1) (2013) 117–128.